Aerodynamic Performance Considerations in the Design of a Coaxial Proprotor

J. Gordon Leishman*
Minta Martin Professor of Engineering
Department of Aerospace Engineering, Glenn L. Martin Institute of Technology
University of Maryland, College Park, MD

Aerodynamic issues in the design of a torque-balanced, contrarotating coaxial proprotor are discussed. A blade element momentum theory (BEMT), formulated to account for the interfering flows in a coaxial rotor system, was validated against performance measurements for a contrarotating coaxial propeller. The BEMT was then used to develop an initial series of blade shapes for a coaxial proprotor, with the goals of maximizing aerodynamic efficiency both in hover (as a pure lifter) and in forward flight (as a pure propulsor). Initially, separate blade performance optimization in hover and in axial flight was undertaken. The BEMT suggested that, besides the normal limiting problems of blade stall and compressibility losses, the overall performance of a coaxial proprotor can be limited by its inability to reach a torque-balanced state. Performance estimations were also supported by results from a free-vortex method, which provided information on the spanwise loads and downstream wake boundaries. A hybrid blade design for the coaxial proprotor was then obtained. The optimum blade twist for the upper proprotor was shown to be of conventional hyperbolic form, whereas the optimum twist on the lower proprotor must have a multipart hyperbolic form. The break points in the twist distributions are related to the average positions of where the wake boundaries from the upper proprotor are assumed to impinge upon the lower proprotor at the specified design conditions in hover and axial flight. The hybrid blade design was shown to give the proprotor good propulsive efficiency while still retaining relatively good hovering performance. The need for a unified composite efficiency metric to properly describe and compare the performance of coaxial proprotors over their entire operational envelope is also discussed.

Nomenclature

A	rotor disk area (for one proprotor), m^2
A_c	contracted slipstream wake area, m^2
a	nondimensional radial wake contraction
C_P	rotor power coefficient, $= P/\rho A\Omega^3 R^3$
C_T	rotor thrust coefficient, $= T/\rho A\Omega^2 R^2$
C_W	weight coefficient, $= W/\rho A\Omega^2 R^2$
C_d	sectional drag coefficient
C_l	sectional lift coefficient
C_{l_α}	sectional lift-curve slope, rad^{-1}
c	blade chord, m
D	propeller diameter, m
F	Prandtl tip loss function
FM	figure of merit
f	exponent in Prandtl tip loss function
J	propeller advance ratio, V_∞/nD
$M_{\Omega R}$	hover tip Mach number
N_b	number of blades
n	revolutions per second
P	rotor power, kW
P_i	induced power, kW
P_0	profile power, kW
R	radius of blade, m
r	nondimensional radial span position
T	rotor thrust, N
V_∞	free-stream velocity, ms^{-1}
v	induced velocity, ms^{-1}
W	vehicle weight, N
y	radial coordinate, m
η	propulsive efficiency
η_c	composite efficiency
θ	blade pitch, rad
λ	nondimensional average inflow velocity, $v/\Omega R$
λ_∞	nondimensional axial velocity, $V_\infty/\Omega R$
ρ	air density, kgm^{-3}
σ	rotor solidity
ϕ	inflow angle
Ω	rotational speed of the proprotor, rad s^{-1}

Subscripts and superscripts

l	lower (or rear) proprotor
u	upper (or front) proprotor

*Corresponding author; email: leishman@umd.edu.
Manuscript received August 2007; accepted September 2008.

Introduction

Various types of advanced convertible rotor concepts continue to be studied in an attempt to develop a rotating-wing aircraft that combines the capabilities of a helicopter (i.e., vertical takeoff and landing with efficient hovering performance) with the capabilities of an airplane (i.e., efficient cruise performance and long-range flight capability carrying high payload). These convertible rotor aircrafts can encompass a broad range of concepts and may not just be limited to the conventional tiltrotor or tiltwing. Such concepts have the potential for use in many military and civil roles, and despite considerable development times and high costs, they may play an increasingly important role in the longer-term future of vertical flight aviation. For example, various types of convertible rotor concepts are contenders to meet the challenging payload, range, and speed requirements of recent military and civil rotorcraft initiatives (e.g., Refs. 1, 2), which demand the carriage of payloads of at least 25 tons over ranges up to 1200 nautical miles. Such high payloads are not exactly new requirements for rotorcraft (Refs. 3–7), but combined with the longer ranges and higher speeds, these requirements pose many engineering challenges in the design of an appropriate vertical lift aircraft.

In an attempt to meet these challenging speed, range, and payload requirements, while still balancing technical risk and containing development costs, the mono tiltrotor (MTR) has been proposed as one possible design solution (Refs. 8–11). Artist illustrations of the MTR are shown in Fig. 1. The MTR is conceptualized as a crane-type of tiltrotor, with an aerodynamically streamlined suspended payload unit. A distinguishing feature of the MTR is that it uses a coaxial proprotor that converts (tilts) from a lifter to a propulsor between vertical flight and forward flight modes, respectively. A relatively high aspect ratio aerodynamically actuated folding wing (Ref. 11) provides lift for efficient cruise in forward flight and which folds down to give minimal vertical download in hovering flight. This wing gives the MTR the lift-to-drag ratios in cruise that are expected to be at least double those of a conventional helicopter and may also exceed those of other competing tiltrotor or tiltwing concepts.

The underpinning of the MTR is its contrarotating coaxial proprotor system, which provides the vertical lift in hover—see Fig. 1(a)—but also tilts forward for cruise flight with the proprotor acting as a propulsor—see Fig. 1(b). The ability to design a coaxial proprotor for efficient hovering flight performance, while still retaining good efficiency as a propulsor, is fundamental to the MTR's success. To this end, the main objective of the present work was to develop a rational basis to initiate the process of designing such a coaxial proprotor system to give acceptable levels of performance over the MTR's projected flight envelope. This type of proprotor may have several design constraints (such as size, disk loading, torque balance issues, maximum allowable downwash, and so on) besides the need to achieve the best aerodynamic performance, so a validated analysis capability was required to explore quickly many design options. The overall goal was to develop an aerodynamic methodology to determine an acceptable set of initial blade designs for the coaxial proprotor that could form candidates for future wind tunnel testing and for the validation of various types of prediction methodologies.

(a) Converting into hover with the proprotors as lifters

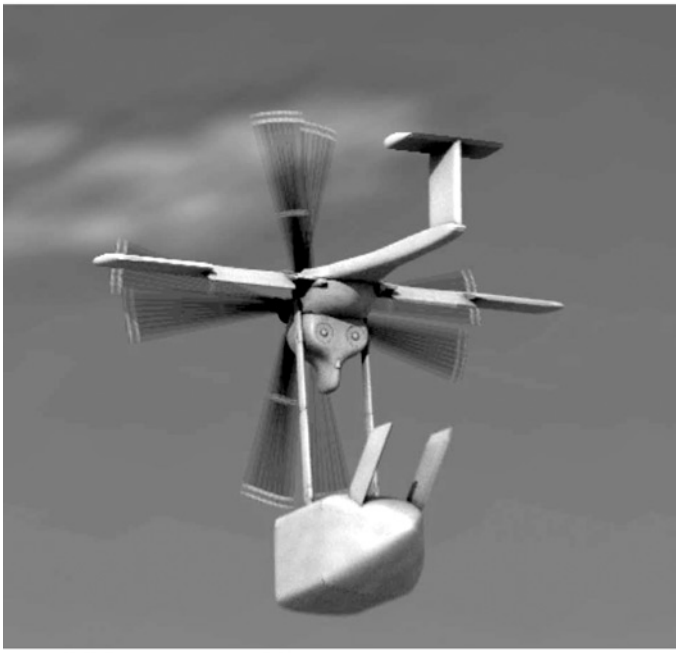

(b) After wing deployment with the proprotors acting as propulsors

Fig. 1. Conceptual sketches of the MTR: (a) MTR converting into hovering flight operation with the proprotors acting as lifters; (b) forward flight with wings and tail fully deployed with proprotors acting as propulsors (images courtesy of Baldwin Technologies LLC).

Analysis of a Coaxial Proprotor

A significant engineering challenge for any convertible rotor concept is the need to design the proprotors to operate efficiently and with sufficient performance margins over a wide range of flight conditions (i.e., in hover through high-speed forward flight, including flight maneuvers in helicopter mode, and so on). The published literature is sparse on proprotor design issues, but it is clear that proprotor performance can be much more compromised than would otherwise be desired (Refs. 12, 13). These problems become especially acute for advanced proprotors that are designed to achieve high-speed forward flight (say, more than 350 kt). Performance measurements on conventional propellers at these conditions have shown narrow margins on their operational efficiency (Refs. 14, 15). It is not unexpected then that any proprotor, which must always retain a high static thrust efficiency in hover, could experience more significantly compromised levels of performance when operated in propeller mode.

Most of the aerodynamic analysis in the present work was conducted using the blade element momentum theory (BEMT) extended to model

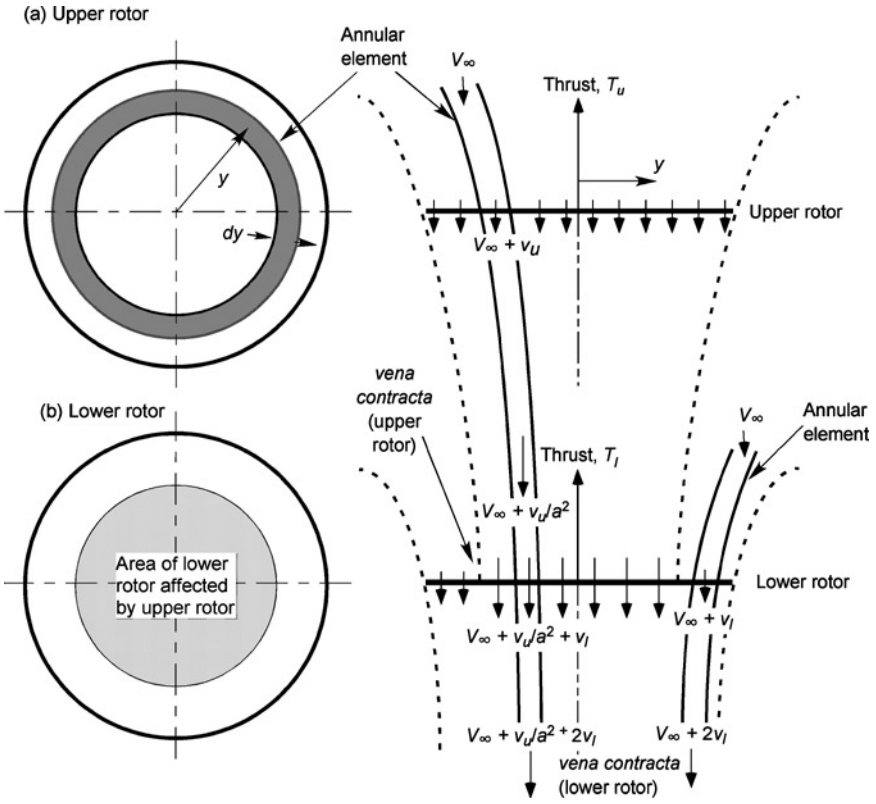

Fig. 2. Flow model used for the BEMT analysis of a coaxial proprotor system with the lower (back) proprotor operating in the slipstream of the upper (front) proprotor.

a coaxial rotor system (Ref. 25). The BEMT is mathematically parsimonious, computationally expedient, and reasonably well validated against various types of rotor and propeller performance measurements. It provides a robust modeling basis from which to initiate a proprotor design solution for further analysis. Studies of coaxial rotor performance using other approaches such as computational fluid dynamics (CFD) are still very limited (Refs. 16–18). Besides all of the usual issues in the preservation of wake vorticity, grid-dependent solutions, etc., the main problem with CFD is one of extremely high computational costs, with Reynolds-averaged Navier–Stokes (RANS) solutions of coaxial rotors (Ref. 17) taking hundreds of hours of computer time to generate a single performance polar. It is not surprising then that CFD approaches have not yet led to any new insights into the better design of coaxial rotors.

The BEMT combines the principles from the blade element and momentum theory approaches and uses the equivalence between the circulation and momentum theories of lift (Refs. 19–22). The flow model used for the coaxial rotor system is shown in Fig. 2, as used in Ref. 25. It is assumed that the lower proprotor operates partly in the fully developed slipstream of the upper proprotor. The BEMT equations are formalized using the assumption that the slipstream wake (outflow) from the upper rotor affects the flow into the lower rotor, but the lower rotor does not produce an induced interference at the upper rotor. This is equivalent to the assumptions made by Lock (Ref. 26) and others (Refs. 27, 28), where the flow velocities of the two rotors are calculated independently and the interference effects are determined by superposition. However, this assumption does not imply that the performance of the upper rotor will be unaffected by the lower rotor; there is always a mutual aerodynamic coupling between the rotors because the inflows and spanwise loading distributions are affected by the overall load sharing and trim state of the coaxial as a system (i.e., for given blade pitch values, thrust sharing, and/or for a torque-balance).

Consider first the upper rotor of the coaxial (see Fig. 2). Assuming the validity of the differential form of the classic momentum theory (Refs. 23, 24), the incremental thrust coefficient acting on the rotor annulus is

$$dC_{T_u} = \frac{dT_u}{\rho(\pi R^2)(\Omega R)^2} = \frac{2\rho(v_u + V_\infty)v_u\, dA}{\rho\pi R^2(\Omega R)^2} = 4\lambda\lambda_u r\, dr \quad (1)$$

where the nondimensional inflow is given by $\lambda = \lambda_u + \lambda_\infty$. Therefore,

$$dC_{T_u} = 4\lambda\lambda_u r\, dr = 4\lambda\,(\lambda - \lambda_\infty)\; r\, dr \quad (2)$$

The induced power coefficient for the annulus is

$$dC_{P_u} = \lambda dC_{T_u} = 4\lambda^2\lambda_u r\, dr = 4\lambda^2\,(\lambda - \lambda_\infty)\, r\, dr \quad (3)$$

to a small angle assumption. This formulation assumes no losses from swirl velocities in the rotor wake, which is justified for lightly loaded rotors of any configuration.

Blade tip loss effects (i.e., the locally high induced losses at the blade tip from the formation of the tip vortex) can be accounted for in the BEMT by using the Prandtl tip-loss function (Ref. 23). This loss is expressed in terms of a correction factor, F, as

$$F = \left(\frac{2}{\pi}\right)\cos^{-1}(\exp(-f)) \quad (4)$$

where f is given in terms of the number of blades, N_b, and the radial position of the blade element, r, by

$$f = \frac{N_b}{2}\left(\frac{1-r}{r\phi}\right) \quad (5)$$

and ϕ is the inflow angle (equal to $\lambda(r)/r$ using a small angle assumption). The Prandtl tip loss function changes the fluid velocity as

it passes through the control volume and modifies the incremental thrust equation to

$$dC_T = 4F\lambda\lambda_u r\, dr \tag{6}$$

Using the conventional blade element theory (i.e., the circulation theory of lift) with the same small angle assumptions, then the incremental thrust produced on the disk is

$$dC_{T_u} = \frac{1}{2}\sigma_u\, C_l r^2\, dr = \frac{1}{2}\sigma_u\, C_{l_\alpha}(\theta_u - \phi) r^2\, dr = \frac{\sigma_u\, C_{l_\alpha}}{2}\left(\theta_u r^2 - \lambda r\right) dr \tag{7}$$

where θ_u is the blade pitch distribution on the upper rotor, which may include the zero-lift angle(s) of the blade sections. Therefore, equating the incremental thrust coefficients derived from the momentum and blade element theories (i.e., using Eqs. (2) and (7)) gives the quadratic equation

$$\lambda^2 + \left(\frac{\sigma_u\, C_{l_\alpha}}{8F} - \lambda_\infty\right)\lambda - \frac{\sigma_u\, C_{l_\alpha}}{8F}\theta_u r = 0 \tag{8}$$

This equation in λ has the solution

$$\lambda(r, \lambda_\infty) = \sqrt{\left(\frac{\sigma_u\, C_{l_\alpha}}{16F} - \frac{\lambda_\infty}{2}\right)^2 + \frac{\sigma_u\, C_{l_\alpha}}{8F}\theta_u r} - \left(\frac{\sigma_u\, C_{l_\alpha}}{16F} - \frac{\lambda_\infty}{2}\right) \tag{9}$$

where $\lambda_u = \lambda - \lambda_\infty$. Equation (9) can be solved numerically over a series of discretized elements that are distributed radially over the rotor blade (Ref. 23). Note that because F is a function of the inflow λ, the inflow equation is normally solved by fixed-point iteration.

The same basic principles can be applied to the analysis of the lower rotor of the coaxial. However, in this case it is assumed that the inner part of the lower rotor operates in the vena contracta of the upper rotor (Fig. 2) with a fully developed slipstream velocity and a maximum change in its axial momentum. The slipstream velocity in the streamtube of the upper rotor can be defined on the basis of an assumed radial contraction of the wake, a, i.e., the contracted wake area is $A_c = \pi a^2 R^2$. In the ideal case then $a = 2^{-1/2} = 0.707$ or $A_c/A = 0.5$. Therefore, the inner area of the lower rotor encounters incoming streamtubes with velocity $V_\infty + 2v_u$, or with velocity $V_\infty + (A/A_c)v_u$ in the more general case where the wake contraction is specified empirically.

For points on the lower rotor disk that are affected by the slipstream generated by the upper rotor (i.e., for values of $r \le a$), the inflow distribution on the lower rotor is given by solving

$$\lambda(r, \lambda_\infty) = \sqrt{\left(\frac{\sigma_l\, C_{l_\alpha}}{16F} - \frac{\lambda_\infty + (A/A_c)\lambda_u}{2}\right)^2 + \frac{\sigma_l\, C_{l_\alpha}}{8F}\theta_l r} - \left(\frac{\sigma_l\, C_{l_\alpha}}{16F} - \frac{\lambda_\infty + (A/A_c)\lambda_u}{2}\right) \quad \text{for } r \le a \tag{10}$$

where θ_l is the blade pitch distribution on the lower rotor and $\lambda_l = \lambda - \lambda_\infty$. For points outside this area that are unaffected by the upper rotor (i.e., for values of $r > a$), the inflow distribution is given by solving

$$\lambda(r, \lambda_\infty) = \sqrt{\left(\frac{\sigma_l\, C_{l_\alpha}}{16F} - \frac{\lambda_\infty}{2}\right)^2 + \frac{\sigma_l\, C_{l_\alpha}}{8F}\theta_l r} - \left(\frac{\sigma_l\, C_{l_\alpha}}{16F} - \frac{\lambda_\infty}{2}\right) \quad \text{for } r > a \tag{11}$$

Note that the contracting streamtubes must be mapped from points on the upper rotor where they are generated to points on the lower rotor within the inner area that is affected by the wake, i.e., the streamtube emanating from radial point r on the upper rotor will map to radial point ar on the lower rotor.

The three inflow equations (Eqs. (9)–(11)) are solved numerically at discrete radial positions over the rotor disks and so give approximations to the inflow at the blades for any specified blade pitch, twist distribution, planform shape (i.e., chord distribution), and airfoil sections (i.e., by varying the airfoil properties through the effects of lift-curve-slope and zero-lift angle of attack). Note that the solutions for the inflow on the upper *and* lower rotors are intrinsically coupled by the trim state of the combined coaxial rotor as a system. When the spanwise inflow distributions are obtained, the rotor thrust and power (with the addition of profile losses) for each rotor may then be found by numerical integration across each respective rotor disk. Normally, in application of the BEMT, the lift and profile drag coefficients, C_l and C_d, in the various equations are replaced by values for specific airfoils by using a table look-up procedure.

The coaxial rotors were normally trimmed (unless otherwise specified) by adjusting their respective reference (collective) pitch angles to meet the specified total system thrust (i.e., using $C_T = C_W = C_{T_u} + C_{T_l}$) or they can be trimmed to any other specified thrust-sharing condition between the upper and lower rotors, as required. Normally, the rotors will be operated at a torque (power) balanced condition (i.e., $C_{P_u} - C_{P_l} = 0$ for equal rotational speeds), where the blade pitch and/or thrust-sharing is *not* assumed a priori, and these become outputs of the trim process.

Validation for a Coaxial Propeller

There have been no performance measurements made on coaxial proprotors, at least not yet. Therefore, the BEMT was validated against measurements made for coaxial contrarotating propellers, which are often known in the literature as tandem propellers or dual-rotation propellers. The BEMT has been previously validated against measurements for a single propeller (Ref. 25), with excellent levels of correlation up to and beyond the onset of supercritical helical tip Mach numbers. Unfortunately, there have been few measurements documenting the performance characteristics of contrarotating propellers at the rotational tip speeds, tip Mach numbers, and tip speed ratios that would be typical of those encountered by a proprotor. The comprehensive results obtained by Biermann and Hartman (Ref. 35), Biermann and Gray (Ref. 36), and Biermann et al. (Ref. 37) are for nominally full-scale contrarotating propellers, but they were operated at subscale rotational tip speeds and tip Mach numbers. However, the tests were conducted at conditions that took the helical Mach numbers on the propeller tips just into the transonic flow region at the higher tip speed ratios. Pairs of two-, three- and four-bladed contrarotating propellers were tested. The pitch of the blades was fixed and was set with an appropriate differential pitch to give an approximate torque-balance near maximum efficiency. Despite the fact that the tests were performed over six decades ago, they are still probably the best available coaxial rotor data for use in validation studies.

The performance of the propeller was examined as a function of the forward speed ratio (also referred to here as the tip speed ratio), which is defined as the ratio of the true axial flow speed, V_∞, to the tip speed of the proprotor, ΩR. Note that propeller performance is conventionally plotted versus "advance ratio" J, so the values of "tip speed ratio" and J are related simply by the formula: tip speed ratio $= J/\pi$.

Figure 3 shows the variation of total thrust on the three-bladed contrarotating propeller pair versus tip speed ratio as a set of curves for increasing values of blade pitch (nominally from 20° upward in steps of 5°). The blade section characteristics were specified using a method similar to that described in Ref. 38 for the Clark Y airfoils used on this propeller, but with the addition of poststall aerodynamic coefficients. From zero forward speed and low blade pitch, the thrust decreases with increasing V_∞. Eventually, the propeller produces negative thrust (i.e., the brake state is reached) unless the blade pitch is subsequently increased to

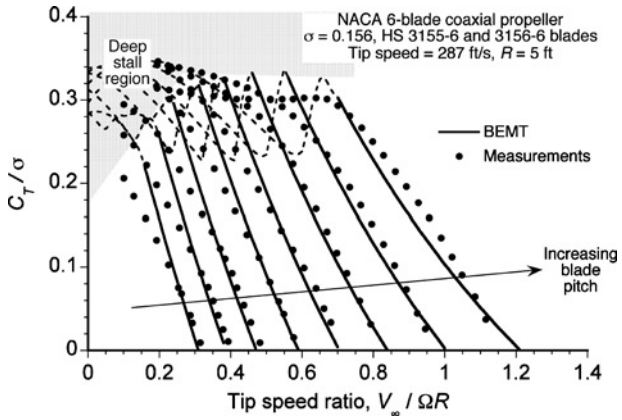

Fig. 3. Validation of the BEMT with thrust measurements for a NACA coaxial propeller as a function of tip speed ratio. Blade pitch is nominally from 20° upward in steps of 5°. (Dashed lines represent predictions with nonlinear aerodynamics and blade stall.)

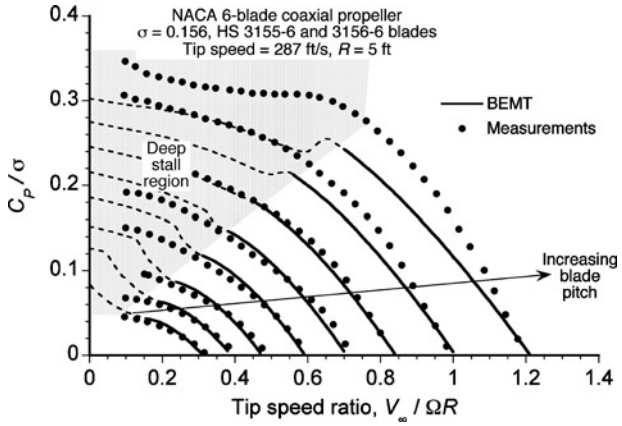

Fig. 4. Validation of the BEMT with power measurements for a NACA coaxial propeller as a function of tip speed ratio. Blade pitch is nominally from 20° upward in steps of 5°. (Dashed lines represent predictions with nonlinear aerodynamics and blade stall.)

higher values. At low forward speeds with higher pitch values the blades are initially stalled, so the propeller generates some thrust but needs high power (see Fig. 4). Increasing V_∞ for a fixed blade pitch and tip speed causes the flow on the blades to attach; thereafter, the propeller produces thrust and the power requirements significantly decrease. Propulsive efficiency also builds rapidly—see Fig. 5. Again, the thrust on the propeller is seen to decrease quickly with V_∞ when the blade pitch is held constant.

The overall success of the BEMT is seen to be relatively good, although there are clearly some deficiencies. These deficiencies are particularly apparent at higher values of C_T/σ and at higher tip speed ratios, where the effects of stall and compressibility both start to manifest. In this case, however, both of these physical effects must be predicted equally well on both the front and rear propellers to achieve overall predictive success.

Figure 4 shows the corresponding predictions of power as a function of tip speed ratio for a range of blade pitch angles. The power curves are relatively sensitive to variations in V_∞ and become steeper at the higher tip speed ratios. This is because the induced losses become a progressively smaller fraction of the total losses, and the curves are

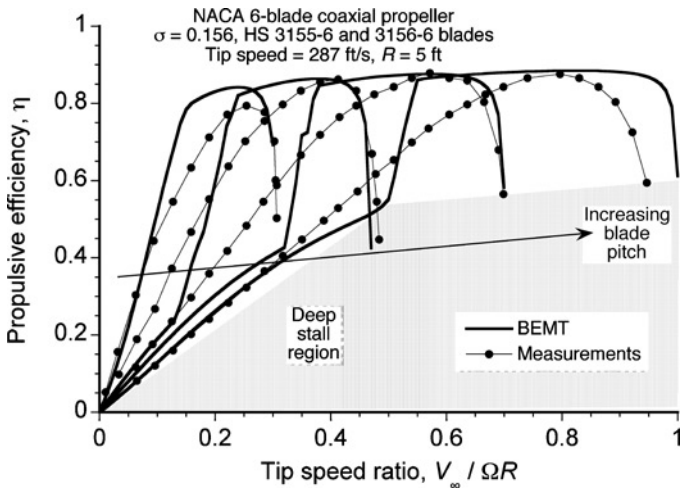

Fig. 5. Validation of the BEMT with propulsive efficiency measurements for a NACA coaxial propeller as a function of tip speed ratio. Blade pitch is nominally from 20° upward in steps of 10°.

defined more by the profile drag on the blades. Predictions of the power are very good at the lower tip speed ratios, but become increasingly less satisfactory at the higher thrusts and as higher tip speed ratios are reached. In this case, there is obviously a need to model more accurately the blade section airloads at higher angles of attack and at higher local Mach numbers. These issues are compounded by the difficulties in actually predicting the angles of attack at the blade elements, which result from rotor-on-rotor interference effects, and this is indeed a challenge for the BEMT with its inherent assumptions and approximations. Another issue is that for these conditions the small angle assumptions made in the previous development of the BEMT equations become increasingly questionable. The present results, therefore, should be interpreted within the bounds set by the approximations made in the development of the theory.

Figure 5 shows predictions of propulsive efficiency, which is defined in the conventional way as

$$\eta = \frac{\text{ideal propulsive power}}{\text{actual shaft power required}} = \frac{T V_\infty}{T V_\infty + P_i + P_0} \tag{12}$$

where T is the net system thrust, P_i is the induced power (including interference losses), and P_0 is the profile power. For a propeller, the induced power becomes a smaller fraction of the total power with increasing V_∞, so that for higher tip speed ratios the minimization of profile losses becomes critical in maintaining good propulsive efficiency. In this case, fewer curves have been shown to preserve clarity. The sensitivity of the propulsive efficiency to small under- or overpredictions of thrust and/or power should be noted. Note also that the measured efficiency curves tend to be fairly peaky compared to the BEMT results, which predicts higher levels of efficiency are obtained over a broader range of operating conditions. Nevertheless, the envelope of peak propulsive efficiency is predicted very well.

The individual efficiency curves are bounded at low tip speed ratios by losses resulting from blade stall; as tip speed ratio increases (for a fixed blade pitch), the flow attaches to the blades and efficiency increases quickly. Note that the measurements suggest a much smoother aerodynamic transition from stalled to attached flow, which would be expected because this flow attachment process is three dimensional in nature compared to that predicted using the two-dimensional airfoil assumptions within the BEMT. On the other side of the peak in efficiency, the shape

of the curve is bounded by the reduction in thrust or the onset of stall (at low tip speed ratios) or growing compressibility effects as the tip sections encounter transonic flow at the higher tip speed ratios. Overall, the BEMT gives an approximate, but reasonably representative, definition of the propulsive efficiency curve, and clearly exposes the issues that will limit the operating efficiency of a contrarotating propeller.

Optimum Hovering Coaxial Proprotor

The confidence established with the BEMT was used to help design a coaxial proprotor to achieve a given level of performance at a given flight condition. These conditions were all at relatively low tip speed ratios where the BEMT (at least in the current incarnation) has been shown to have better validity. In the first instance, the static thrust (i.e., hovering) efficiency was addressed. This was followed by an analysis of the optimum blade shape to give the proprotor its maximum propulsive efficiency. It should be appreciated that the resulting blade shapes will always be a point design—the amount and spanwise distributions of twist, as well as the blade planform for each proprotor, will depend on the operating states of the proprotors, i.e., on C_T and V_∞, as well as the thrust-sharing level at the torque-balanced state.

The design process starts with the specification of the system thrust (i.e., $C_T = C_W$ in hover) and the requirement for either an equal thrust sharing (i.e., $C_{T_u} = C_{T_l} = C_W/2$) or a net torque-balance on the two proprotors (i.e., $C_{P_u} - C_{P_l} = 0$). By means of a separate sizing study (Refs. 8, 9), a proprotor with five blades and solidity of 0.129 per rotor at total $C_T = 0.016$ in hovering flight was considered as an initial design. The loads on the upper proprotor are then determined using the BEMT from an initially presumed distribution of $\theta_u(r)$ and so finding a first solution for the inflow distribution $\lambda_u(r)$. The thrust distribution dC_{T_u}/dr is then determined, and the thrust C_{T_u} and power C_{P_u} on the upper rotor are found by radial integration. Uniform disk loading is then achieved by finding the distribution of $\theta_u(r)$ such that $dC_{T_u}/dr = 2C_{T_u}$. This inflow $\lambda_u(r)$ then defines the upstream flow into the lower proprotor, from which the inflow $\lambda_l(r)$ is determined by solving Eqs. (10) and (11), while imposing a linear thrust distribution for optimum performance, i.e., in this case by setting $dC_{T_l}/dr = 2C_{T_l}$. This requirement gives uniform disk loading on the lower proprotor but note that this is not achieved with uniform inflow throughout; uniform inflow distributions are obtained over the inner and outer regions of the lower proprotor disk but they have different magnitudes. The trim process then continues by finding the new distributions of θ_u and θ_l to give a torque-balance on the two proprotors (finding $C_{P_u} - C_{P_l} = 0$ to within a 0.05% error was found to be sufficient) while relaxing the need for equal thrust sharing.

The blade pitch to achieve the best hovering efficiency of this coaxial proprotor at the specified operating point is shown in Fig. 6. In this case, airfoil characteristics for the NACA 0012 were assumed. The tip Mach number was 0.65. Clearly the amount of blade twist required is considerable, with the twist angles approaching 40° (between the tip and an assumed root cutout at $r = 0.15$) on the lower proprotor. Note that a considerably larger amount of blade twist is needed on the lower proprotor to compensate for the high outflow velocities induced by the upper proprotor. Outside the influence of the slipstream boundary, the blade pitch requirements are reduced considerably.

The predicted figure of merit of this proprotor is shown in Fig. 7. The results are given for the upper proprotor, the lower proprotor, and for the coaxial as a system. Note that the calculations have been carried out until the proprotors begin to stall; the onset of stall causes a loss in thrust and an increase in power requirements, so substantially reducing the *FM*. The definition of *FM* that is based on total system thrust (see the definition discussed by Coleman in Ref. 31) produces a fictitiously high value of overall system efficiency because it assumes that both

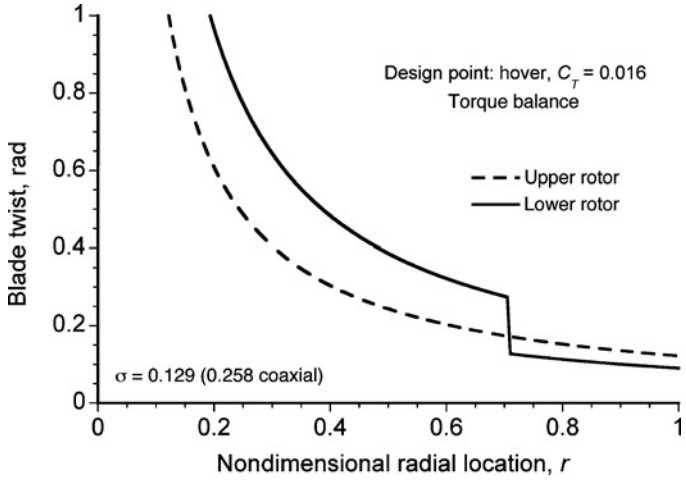

Fig. 6. Optimized blade twist distribution for the upper and lower proprotors at the specified hovering design point. Ideal wake contraction for the upper proprotor is assumed.

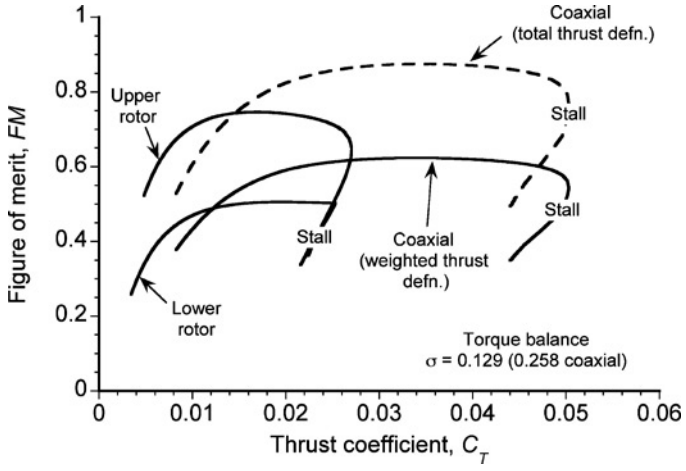

Fig. 7. Figure of merit versus thrust coefficient for the optimized proprotor in hovering flight.

of the rotors operate at twice their actual disk loadings. Therefore, for the purposes of performance evaluation, a weighted thrust definition of *FM* has been deemed more appropriate and was used in this study by assuming that each rotor of the coaxial operates with equal thrust sharing (i.e., $T_u = T_l = W/2$). In this case, the ideal power for the two rotors free of interference effects can be written as

$$P_{\text{ideal}} = \frac{T_u^{3/2}}{\sqrt{2\rho A}} + \frac{T_l^{3/2}}{\sqrt{2\rho A}} = \frac{\left(\frac{W}{2}\right)^{3/2}}{\sqrt{2\rho A}} + \frac{\left(\frac{W}{2}\right)^{3/2}}{\sqrt{2\rho A}} = 2\frac{\left(\frac{W}{2}\right)^{3/2}}{\sqrt{2\rho A}} = \frac{W^{3/2}}{\sqrt{4\rho A}} \tag{13}$$

In terms of system power, C_P, then this alternative definition of the *FM* becomes

$$FM = \frac{C_W^{3/2}}{2\,C_P} \tag{14}$$

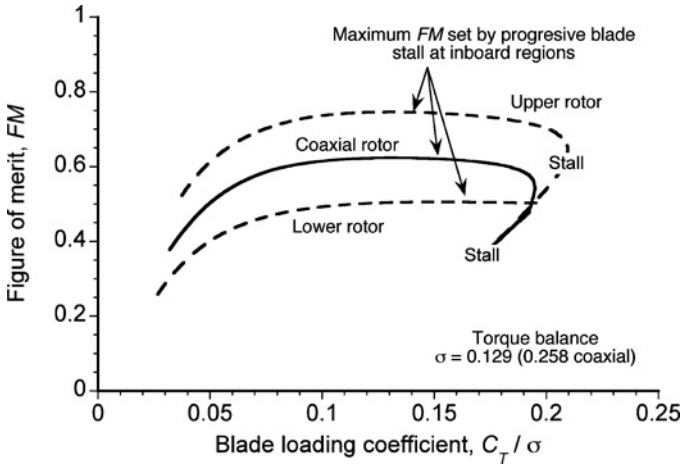

Fig. 8. Figure of merit versus blade loading coefficient for the optimized proprotor in hovering flight.

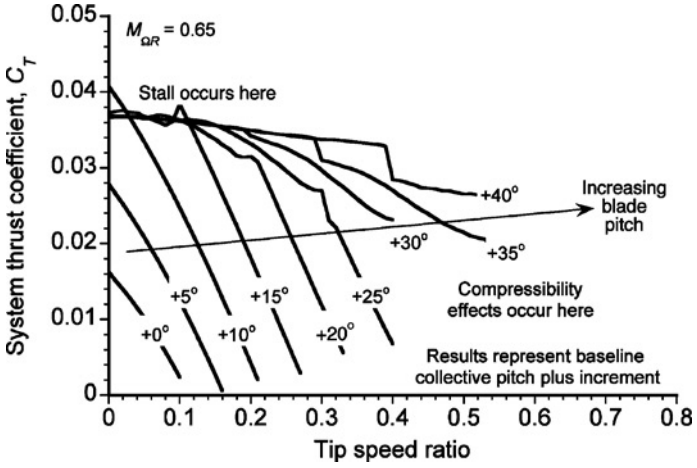

Fig. 9. Predicted variation of the proprotor system thrust versus tip speed ratio for the baseline "ideal" coaxial proprotor optimized for hovering performance.

which is called here the "weighted thrust definition" of *FM*. However, this metric too is based only on an approximation to the actual operating state and aerodynamic efficiencies of the individual proprotors, but it is considered a better metric for comparisons than with using the previous definition. Further details of how *FM* is more appropriately defined for a coaxial rotor are discussed in Ref. 29.

An alternative presentation is to examine the *FM* versus blade loading coefficient, C_T/σ, as shown in Fig. 8. Because the values of C_T/σ are proportional to the average lift coefficients produced on the proprotors, this plot shows that the maximum achievable *FM* (however it is ultimately defined) of the coaxial as a system is determined by the onset of stall on the upper proprotor, although only marginally so in this case. On the upper proprotor, the onset of stall occurs at $C_T/\sigma \approx 0.14$, whereas on the lower proprotor the effects of stall become apparent at $C_T/\sigma \approx 0.155$. This behavior is reflected in the *FM* curves of each individual proprotor, which reach a peak and drop precipitously when stall progresses over a larger proportion of the blades. Interestingly, the stall margins for the coaxial proprotor as a system are found to be set by the stall margins of the upper proprotor, which carries a higher fraction of the total system thrust. This result suggests that to maximize overall stall margins, the upper proprotor may need a larger solidity than the lower proprotor to equalize the stall margins so that neither proprotor by itself will limit overall performance.

Axial flight performance

The performance of the coaxial proprotor was calculated for a series of increasing values of collective pitch over a range of tip speed ratios, as in the manner described previously for the validation exercise. Results for the system thrust coefficient are shown in Fig. 9 using the blade twist distribution that was derived for hovering flight, and with the assumption of a wake contraction ratio of 0.82 from the upper rotor. Recall that this particular proprotor was designed for hovering flight (i.e., to produce a high static thrust efficiency), and not specifically to achieve high propulsive efficiency. It can be seen that the initial range of acceptable performance is bounded by blade stall (high blade pitch at low tip speed ratios) and by the generation of negative thrust (which is obtained at higher tip speed ratios at lower blade pitch values). The relationship between C_T and tip speed ratio is seen to be almost linear in the normal working state of the proprotor (see also Fig. 3).

For proprotors that initially operate with large blade pitch angles at low tip speed ratios, the blades will be stalled. The flow will then attach as tip speed ratio increases, and C_T will then decrease almost linearly with increasing tip speed ratio until the brake state is encountered at a given blade pitch. For higher tip speed ratios, the performance of the proprotor will be degraded because of increasing compressibility losses. Note that the resultant helical velocity of the blade element defines the incident Mach number. Therefore, as forward speed increases, compressibility effects become important when the helical Mach numbers begin to exceed the drag divergence Mach number of the airfoils being used.

What is apparent in this case is that blade stall and/or compressibility effects will limit the overall performance of the proprotor system at relatively low tip speed ratios, and at substantially lower values than would be needed for efficient propulsion in axial flight. This result is better shown in Fig. 10. Note that fairly characteristic propeller efficiency plots are obtained at low collective pitch and low tip speed ratios. The curves show a rapid increase in efficiency, followed by a sharp drop as C_T decreases above a certain value of tip speed ratio. At higher collective pitch angles, blade stall substantially reduces proprotor efficiency, and the curves then follow the blade stall/poststall boundary until a sufficiently high tip speed ratio is reached, where the flow then attaches to the blades. The efficiency curves show an increase in performance until being limited

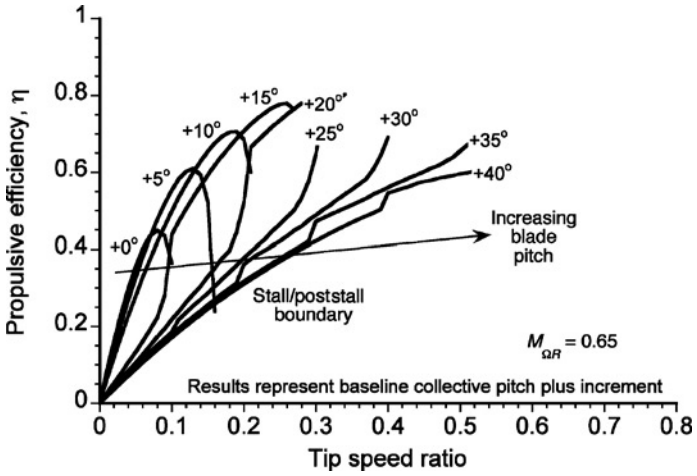

Fig. 10. Predicted variation of propulsive efficiency versus tip speed ratio for baseline "ideal" coaxial proprotor optimized for hovering performance.

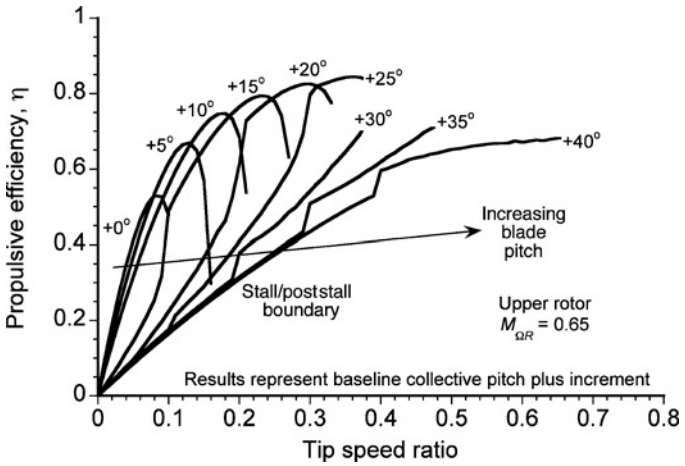

Fig. 11. Predicted variation of propulsive efficiency versus tip speed ratio for the upper (front) proprotor of the baseline "ideal" coaxial proprotor optimized for hovering performance.

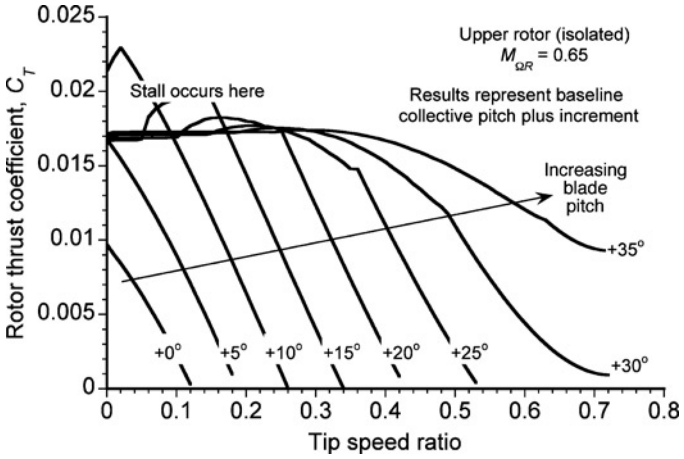

Fig. 13. Predicted variation of the proprotor system thrust versus tip speed ratio for the upper (back) isolated "ideal" coaxial proprotor optimized for hovering performance.

by decreasing thrust, drag rise from compressibility, or because a torque-balance between the upper (front) and lower (back) proprotors cannot be achieved. In this particular case, the limits were reached at relatively low tip speed ratios (i.e., at only 0.3–0.4).

The problems of limiting performance can be better exposed by examining individually the propulsive efficiency of both proprotors, as shown in Figs. 11 and 12. The propulsive efficiency of the upper (front) proprotor is defined by

$$\eta_u = \frac{T_u V_\infty}{T_u V_\infty + P_{i_u} + P_{0_u}} \tag{15}$$

and for the lower (back) proprotor the efficiency is

$$\eta_l = \frac{T_l V_\infty}{T_l V_\infty + P_{i_l} + P_{0_l}} \tag{16}$$

Clearly, the upper (front) proprotor behaves quite typically in terms of performance (i.e., compared to a standard single propeller) until higher collective pitches are reached. Thereafter, the net system efficiency is dictated by the propensity of the lower (back) proprotor to remain stalled until a tip speed ratio of about 0.2 is reached. When the lower (back) proprotor does unstall as tip speed ratio is increased, the propulsive efficiency of the system increases rapidly. However, as the efficiency of the lower (back) proprotor increases, the upper proprotor also reaches its maximum efficiency. Therefore, further system performance becomes limited by decreasing thrust and by the onset of compressibility losses on the upper proprotor. Beyond this point, a torque-balance cannot be achieved, and so the overall performance of the coaxial as a system becomes adversely affected.

It was not immediately obvious that a failure to achieve a torque-balance could prematurely limit the performance of a coaxial proprotor, but the present results suggest that this can indeed occur. This limiting behavior can be better understood by plotting the thrust and propulsive efficiency of the isolated upper proprotor, which are results shown in Figs. 13 and 14, respectively. Note that the isolated upper (front) proprotor can operate efficiently over a much wider range of operating conditions than when it is aerodynamically coupled to the lower (back) proprotor through the need for a torque-balance (cf. Fig. 11). Efficient operation is possible up to tip speed ratios exceeding 0.5 in this case. This

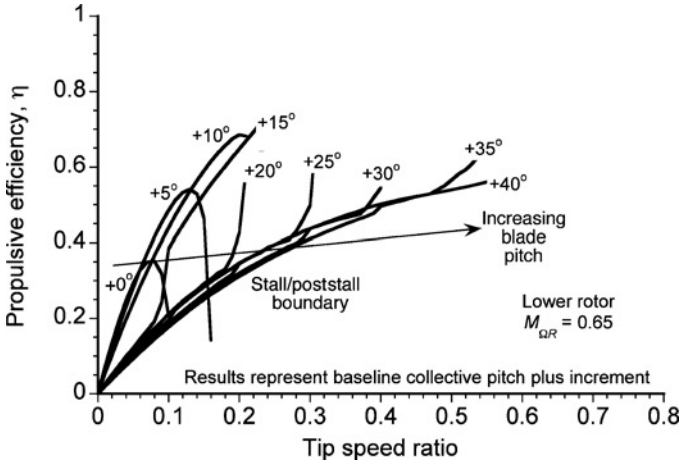

Fig. 12. Predicted variation of propulsive efficiency versus tip speed ratio for the lower (back) proprotor of the baseline "ideal" coaxial proprotor optimized for hovering performance.

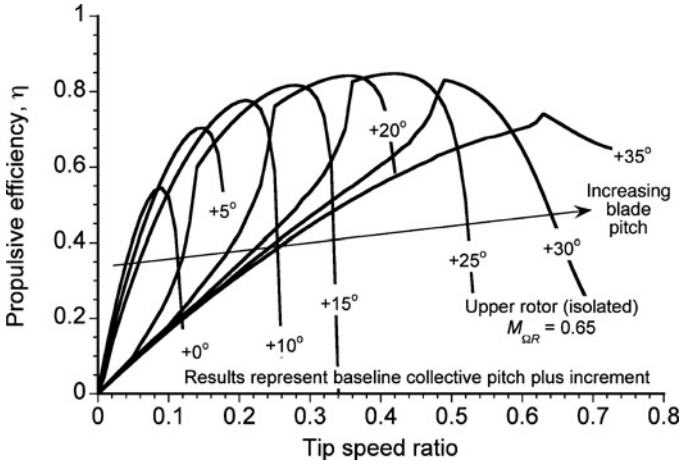

Fig. 14. Predicted variation of propulsive efficiency versus tip speed ratio for baseline upper isolated "ideal" coaxial proprotor optimized for hovering performance.

result is compared to the performance of the same proprotor as part of a coaxial system, where efficient operation is possible only up to tip speed ratios of between 0.3 and 0.4. Beyond this point, the loss of aerodynamic efficiency of one or other of the proprotors, or the inability to achieve a torque-balance, will limit the net propulsive efficiency of the system. This issue shows how the "optimum" design of a coaxial proprotor can become considerably more difficult than for a single proprotor.

Optimum coaxial proprotor in axial flight

It is apparent that a coaxial proprotor system that is designed for maximum hovering efficiency (i.e., for static thrust efficiency) cannot function efficiently as a propulsor in axial flight over the required range of thrusts and tip speed ratios, although this result is perhaps not so surprising based on the discussion in Ref. 12. Therefore, a new blade design solution must be sought. Again, this design must be obtained based on the need to maintain a torque-balanced state between the two proprotors, which is a requirement that can also constrain the number of possible geometric solutions.

In the cruise condition, the thrust of a proprotor will be lower than that required for hovering flight. For an initial high-speed cruise specification, an "ideal" proprotor was designed for a net system C_T of 0.008 at a tip speed ratio of 0.5. The wake contraction ratio from the upper proprotor under these conditions was found (from a free-vortex method or FVM—see Refs. 32–34) to be substantially smaller (i.e., $a = 0.95$) than found for hovering flight (i.e., $a = 0.82$), so the former was used for the design optimization—see Figs. 15 and 16.

In axial flight, the optimum aerodynamic solution for lowest induced power losses is still a uniform disk loading over both the upper and lower proprotors. However, in axial flight the induced velocity becomes a much smaller part of the total inflow through the proprotor as a system. Therefore, the distributions of blade twist on the upper and lower proprotors become more similar and approach single hyperbolic forms. However, it is obvious that the blade pitch distributions needed on both proprotors must be different to those needed in hovering flight.

The results are shown in Fig. 17, where the "ideal" blade pitch distributions are plotted for both the hover and axial flight conditions at their respective design points. Recall that the assumed wake contraction in hover and in axial flight is different (i.e., $a = 0.82$ versus 0.95, respectively), so the discontinuity in the blade twist distribution on the lower (back) proprotor now occurs at a different spanwise location. Note also that because of the smaller induced velocity through the proprotor in axial flight, the change in blade pitch needed at the outer span is substantially smaller than for the axial flight case. This result is important when it comes to the compromise needed in blade design to match the requirements of efficient hovering flight (i.e., in obtaining high values *FM* and good power loading) and for efficient axial flight (i.e., obtaining high vales of η and corresponding good power loading).

The performance of this optimized blade design in axial flight is shown in Fig. 18. Note that the proprotor operates efficiently around its design point at a tip speed ratio of 0.5, as would be expected. Propulsive performance degrades for tip speed ratios above 0.7, mainly because of compressibility losses with the onset of drag rise and the loss of lift resulting from the growing helical tip Mach numbers. These effects, of course, are ameliorated if the rotor tip speed (ΩR) can be reduced through mechanical design, but this also increases the tip speed ratio. Nevertheless, it

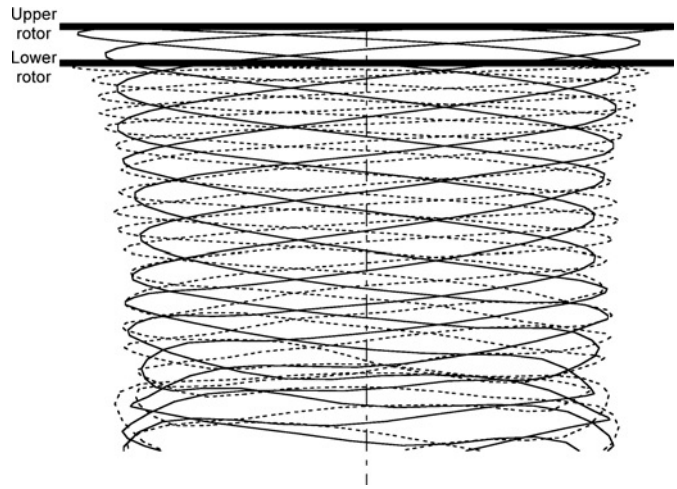

Fig. 15. Representative wake solution from the FVM for the coaxial proprotor in the hover condition.

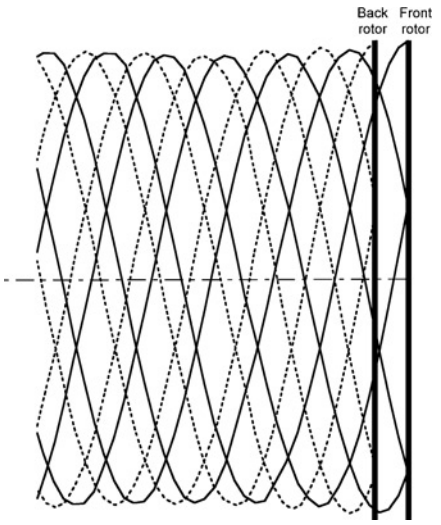

Fig. 16. Representative wake solution from the FVM for the coaxial proprotor in the axial flight condition.

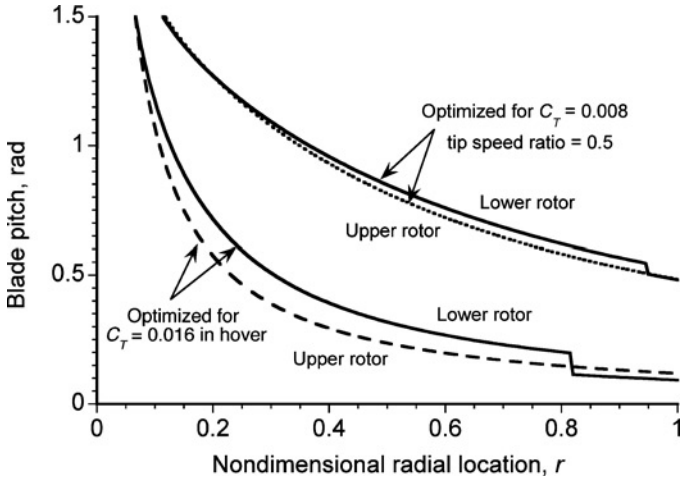

Fig. 17. Optimum or "ideal" distribution of local blade pitch on the coaxial proprotor system in axial flight with design point for $C_T = 0.008$ and tip speed ratio of 0.5.

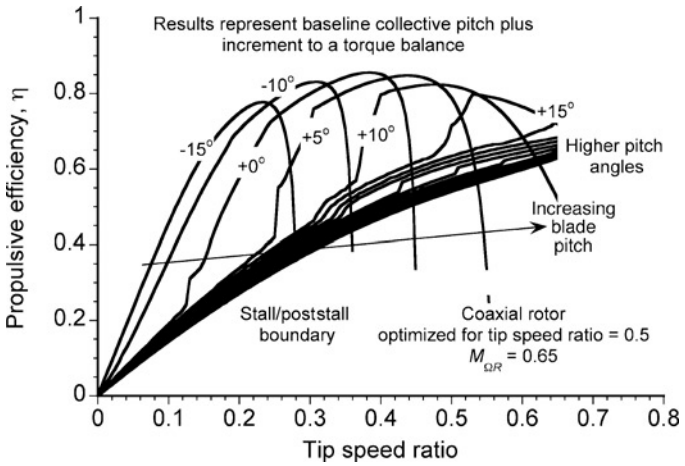

Fig. 18. Predicted variation of propulsive efficiency versus tip speed ratio for the coaxial proprotor system in axial flight with design point $C_T = 0.008$ at a tip speed ratio of 0.5.

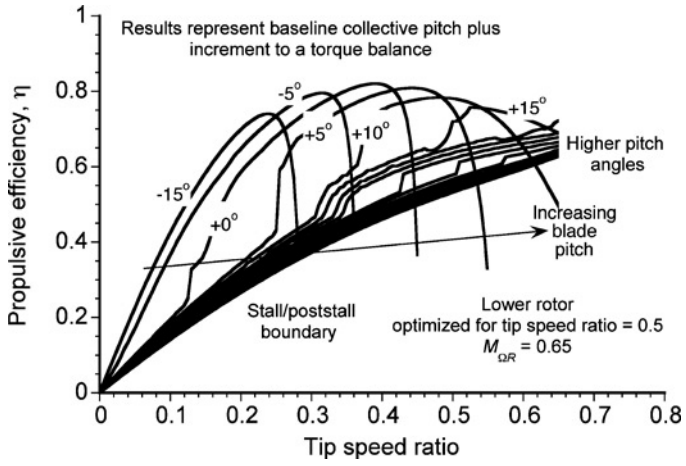

Fig. 20. Predicted variation of propulsive efficiency versus tip speed ratio for the lower (back) proprotor of the coaxial system in axial forward flight with design point $C_T = 0.008$ and a tip speed ratio of 0.5.

is apparent that the operational performance and efficiency of the coaxial proprotor is now substantially better than was obtained for the baseline (hover) design.

In this case, it was found that the upper (front) and lower (back) proprotors operated with a more balanced aerodynamic performance, so that their relative propulsive efficiencies are now very similar—see Figs. 19 and 20. While the upper proprotor still demonstrated a slightly higher relative propulsive efficiency, and also a better efficiency over a wider range of conditions (i.e., for ranges of collective pitch and tip speed ratios), the off-design performance is still somewhat compromised. This "optimized" proprotor design, however, still provides a reasonable level of hovering performance, as shown in Fig. 21, although the range of conditions where a torque-balance can be obtained without blade stall is still more limited than was obtained with the hover-optimized design. Stall margins for this proprotor are also significantly reduced, with the obvious conclusion that this proprotor will not be acceptable to simultaneously meet both axial and hovering flight requirements.

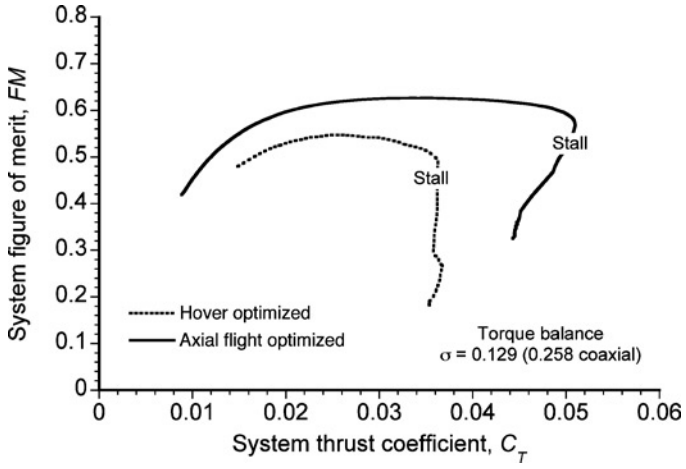

Fig. 21. Hovering system figure of merit for the coaxial proprotor system optimized for axial forward flight.

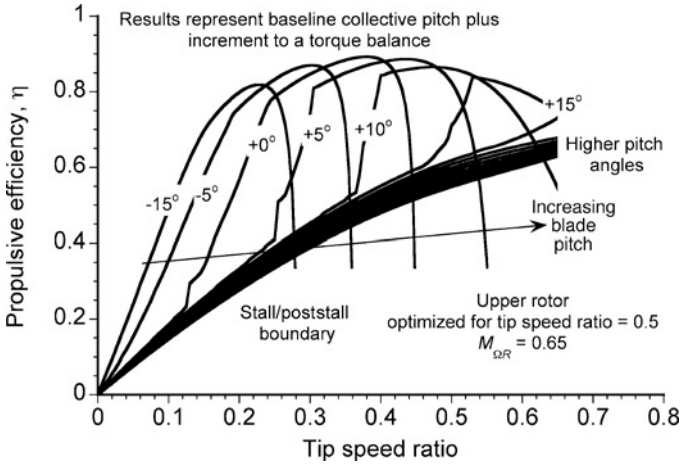

Fig. 19. Predicted variation of propulsive efficiency versus tip speed ratio for the upper (front) proprotor of the coaxial system in axial forward flight with design point $C_T = 0.008$ at a tip speed ratio of 0.5.

Hybrid optimum coaxial proprotor blade design

The foregoing results show that some form of "hybrid" blade design will be necessary to maximize the performance in both hover and in axial flight. While several possibilities were examined, a hybrid blade pitch was selected that was a geometrically weighted average between the optimum ("ideal") values determined for the upper (front) and lower (back) proprotors at the design points in hovering and axial flight, respectively. While this is not a true aerodynamic optimum, in the sense that the blade pitch is designed from the onset to meet the thrust and efficiency requirements of both hover and axial flight while also maintaining a torque-balance, the results subsequently obtained were sufficiently convincing to justify this approach, at least as a first step toward giving blade designs that had more balanced hover and propulsive efficiencies.

Figure 22 shows an example of a hybrid blade design, which in this case is equally geometrically weighted between the optimum blade pitch values found for each proprotor in hover and axial flight at each respective design point. First, note the hybrid design has a different blade twist rate per unit length than for the optimum hovering case. Second, the step

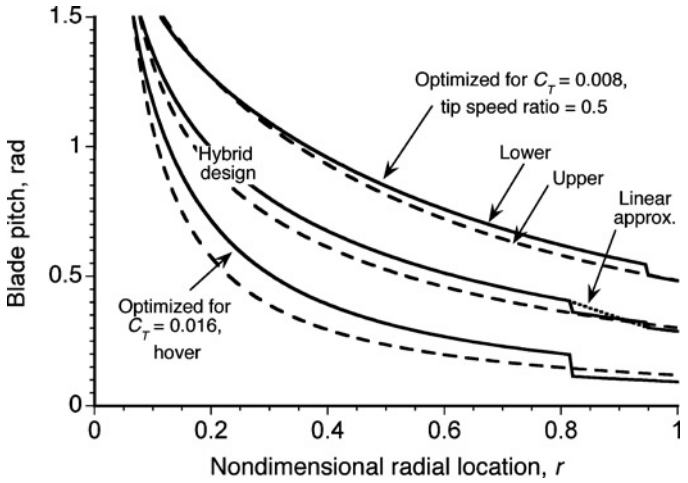

Fig. 22. Distribution of local blade pitch for the hybrid coaxial proprotor system at the design point.

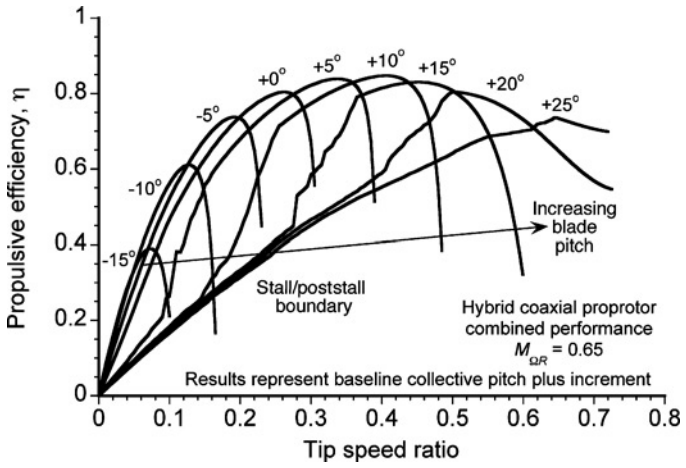

Fig. 24. Predicted variation of propulsive efficiency versus tip speed ratio for the coaxial proprotor system with the hybrid blade twist design.

change in the twist rate on the lower (back) proprotor is substantially reduced, although now two smaller step changes in blade twist are produced. However, as also shown in Fig. 22, these step changes could be easily approximated by some blended distributions for manufacturing purposes; linear approximations are an obvious choice.

The hovering performance of the proprotor system with the hybrid blade geometry is shown in Fig. 23. While showing a small decrease in maximum system *FM* relative to the proprotor system that was optimized for hovering flight, it is clear that the *FM* is substantially better than for the proprotor that was optimized for axial flight alone, as might be expected. Furthermore, the net decrease in stall margins, while still significant, is now more acceptable.

The most noticeable improvements with the hybrid blade design occurs in axial flight, as shown in Fig. 24 in terms of propulsive efficiency versus tip speed ratio. Note the much wider range of acceptable operating conditions compared to either the baseline hovering design (cf. Fig. 10) or the axial flight design (cf. Fig. 18). This outcome occurs because both proprotors of the coaxial system now demonstrate a more balanced aerodynamic performance (as shown in Figs. 25 and 26) with neither of the proprotors by themselves significantly limiting overall system

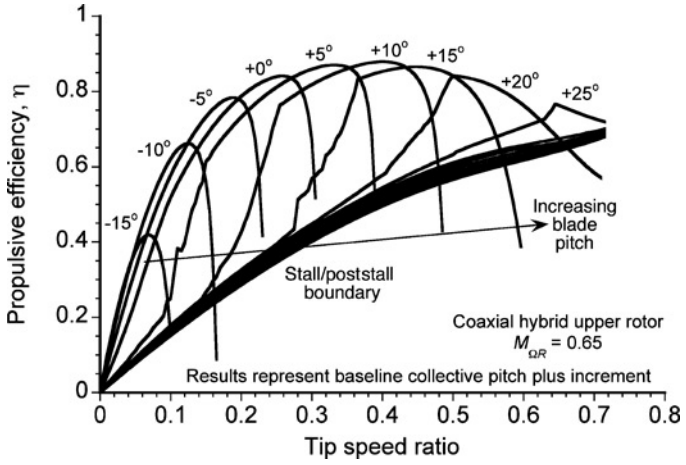

Fig. 25. Predicted variation of propulsive efficiency versus tip speed ratio for the upper (back) proprotor of the coaxial system with the hybrid blade design.

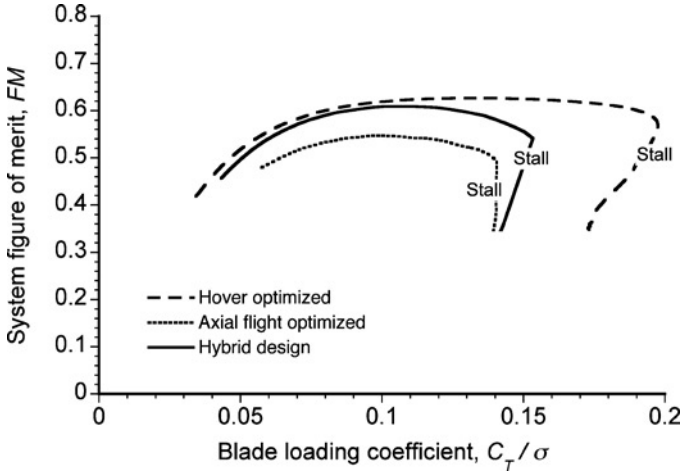

Fig. 23. Hovering system figure of merit for the coaxial proprotor system with the hybrid blade design.

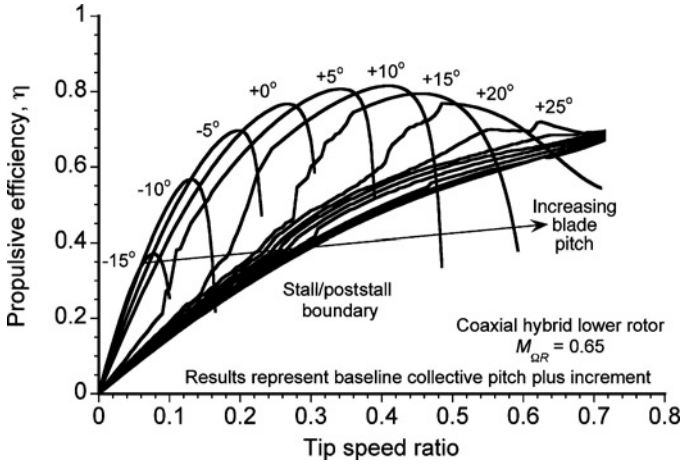

Fig. 26. Predicted variation of propulsive efficiency versus tip speed ratio for the lower proprotor of the coaxial system with the hybrid blade design.

performance. The front proprotor operates with a slightly higher efficiency, as would be expected.

The onset of compressibility losses at the higher helical Mach numbers and higher tip speed ratios eventually leads to significant increases in power required, and so precipitous reductions in overall propulsive efficiency are a result. A net propulsive efficiency of 80% up to a tip speed ratio of 0.6 was considered acceptably good performance to meet the initial design requirements of the MTR, although further improvements in overall aerodynamic efficiency are likely to be possible. To this end, these further improvements will come from the combined design of the blade planform and airfoil sections so as to more optimally distribute the local lift coefficients on both proprotors such that they operate at their best sectional lift-to-drag ratios and also will achieve the necessary high drag divergence Mach numbers, at the correct combinations of incident Reynolds numbers and Mach numbers.

As previously described, the distribution of lift coefficients over the blade is of significant importance in the design of an optimum proprotor system. Representative results for hovering flight are shown in Fig. 27. The need for uniform inflow to give low induced power losses results in high values of blade pitch being needed inboard on the blades, and so higher angles of attack and higher lift coefficients are also produced here. This means that some taper of the blade planform will be required to redistribute the lift coefficients so that the inboard blade sections will remain below stall (also with some margin at the design condition), and also so that they can operate closer to their local maximum lift-to-drag ratios to minimize profile losses.

Note from Fig. 27 that some blade taper reduces the inboard lift coefficients; a 2:1 taper provides an acceptable reduction so that more of the inboard blade sections should remain below stall. Although much depends on the airfoils that are ultimately chosen for the inboard regions of the blade, it is realistic to expect maximum lift coefficients of at least 1.65 using state-of-the-art airfoil design methods. With a typical root cutout of 15% of blade radius, it is apparent that this particular proprotor at least should not be stall limited at its design condition, although stall will still propagate outboard on the blades as thrust demands increase. Stall margins, therefore, still need to be carefully addressed in any final design.

Note also from the results in Fig. 27 that both proprotors operate at different average lift coefficients, another point previously alluded to. Because the need for a torque-balance, the upper proprotor generates a higher fraction of the total system thrust. This means that the upper proprotor will dictate the stall margins for the coaxial proprotor as a whole, and it will be more limited in its aerodynamic performance than if both proprotors had simultaneously reached their stall limits. This problem can only be ameliorated if the average weighted solidity for the upper (front) proprotor is slightly increased and the solidity for the lower (back) proprotor is slightly decreased, although this may not be a practical design solution. Nevertheless, contrarotating propellers with different numbers of blades and solidities on the front and rear propellers have been tested (Ref. 39), and obviously further work must be done to fully understand the design trades.

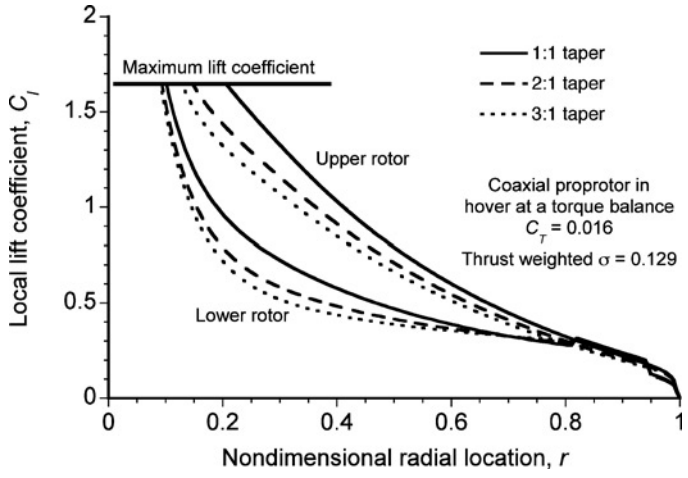

Fig. 27. Variation of the spanwise distribution of local lift coefficient for the coaxial proprotor system with the hybrid blade design with different amounts of linear blade taper operating in hover.

Composite efficiency metric for a coaxial

The efficiency of a coaxial proprotor has been previously evaluated in this paper using two separate metrics: (1) a figure of merit in hover and (2) a propulsive efficiency in forward flight. However, an outcome of this study has shown the need to define more appropriate metrics for the accurate performance evaluation of coaxial proprotors. While an alternative efficiency metric for hover based on thrust sharing has been used in the present work, the primary issue in any definition of the hovering figure of merit is that it has no validity in axial flight. Furthermore, the difficulty with the conventional propulsive efficiency as a metric is that it quickly approaches zero for low tip speed ratios, and so can give a false impression of aerodynamic efficiency at lower axial flight speeds.

To overcome these issues, a composite efficiency metric can be defined in terms of the ratio of ideal power required for flight to the actual power required. For a coaxial proprotor system operating at a torque-balanced condition, the upper and lower proprotors carry an unequal fraction of the total thrust, so any valid efficiency metric must take this reality into account. A composite efficiency metric for a coaxial proprotor can be defined as

$$\eta_c = \frac{\text{ideal power}}{\text{actual shaft power required}} = \frac{T V_\infty + P_{\text{ideal}_u} + P_{\text{ideal}_l}}{T V_\infty + P_{i_u} + P_{0_u} + P_{i_l} + P_{0_l}} \tag{17}$$

where P_{ideal_u} represents the ideal power required for the isolated upper proprotor and P_{ideal_l} is the ideal power for the isolated lower proprotor. The terms P_{i_u} and P_{0_u} are, respectively, the actual induced and profile power values for the upper proprotor, and P_{i_l} and P_{0_l} are the corresponding values for the lower proprotor. In terms of nondimensional coefficients, η_c can be written as

$$\eta_c = \frac{C_T \lambda_\infty + C_{P_{\text{ideal}_u}} + C_{P_{\text{ideal}_l}}}{C_T \lambda_\infty + C_{P_{i_u}} + C_{P_{0_u}} + C_{P_{i_l}} + C_{P_{0_l}}} \tag{18}$$

The ideal power is a function of the tip speed ratio and can be calculated using the simple momentum theory (i.e., no losses other than induced losses). For the isolated upper proprotor, the ideal power coefficient can be written as

$$C_{P_{\text{ideal}_u}} = C_{T_u}\left(\frac{1}{2}\sqrt{\lambda_\infty^2 + 2C_{T_u}} - \frac{\lambda_\infty}{2}\right) \tag{19}$$

and for the isolated lower proprotor it is

$$C_{P_{\text{ideal}_l}} = C_{T_l}\left(\frac{1}{2}\sqrt{\lambda_\infty^2 + 2C_{T_l}} - \frac{\lambda_\infty}{2}\right) \tag{20}$$

The results for the composite efficiency using the proprotor with the hybrid blade twist distributions are shown in Fig. 28. Note that in this

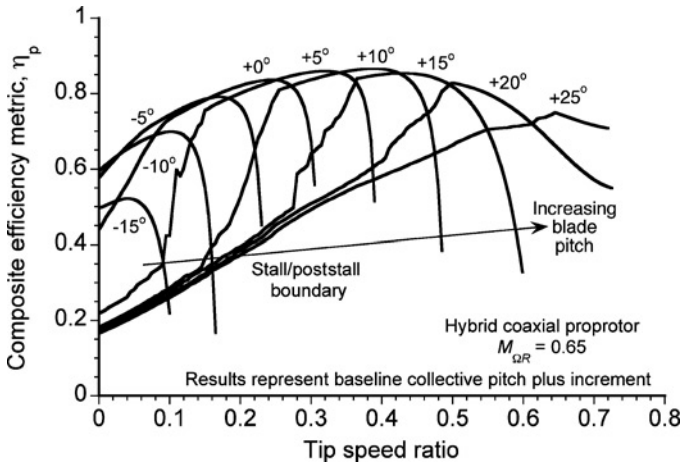

Fig. 28. Variation of the composite efficiency metric versus tip speed ratio for the coaxial proprotor system with the hybrid blade designs.

case, as tip speed ratio approaches zero the composite efficiency approaches the figure of merit for hovering flight (see Fig. 23). At higher tip speed ratios, the composite efficiency approaches the propulsive efficiency (see Fig. 24). Therefore, this approach provides a single metric to help evaluate the performance of candidate coaxial proprotor designs, although further work must be done to verify the more general validity of this or any other such efficiency metric.

Conclusions

Some issues in the aerodynamic design of a torque-balanced, coaxial proprotor have been discussed. An extension of the BEMT to a coaxial rotor was validated against measurements for a contrarotating propeller. The BEMT was then used to design the blade shapes for a coaxial proprotor to give a balanced aerodynamic efficiency in both hover and forward (axial) flight. The following conclusions have been drawn:

1) The optimum case for minimum induced losses and best aerodynamic efficiency occurs when both the upper (front) and lower (back) proprotors operate with uniform disk loadings at a torque-balanced state. The required blade twist for the upper proprotor was shown to be of conventional hyperbolic form, but the lower proprotor must have a multipart hyperbolic blade twist to produce the desired optimum aerodynamic loading. The break points in the blade twist distribution must be related to the average positions of where the wake boundaries from the upper proprotor impinge upon the lower proprotor at the design points in hover and axial flight.

2) The BEMT suggested that besides blade stall and compressibility losses, the overall performance of a nonoptimized coaxial proprotor can be limited by its inability to reach a torque-balanced operating state. It has been shown in this article that "hybrid" blade shapes for both the upper (front) and lower (back) proprotors can be successfully designed such that the resulting proprotor design need not be torque limited and can give an acceptable hovering figure of merit as well as excellent propulsive efficiency.

3) The results have also shown that as a result of interference effects both proprotors of a coaxial can operate at significantly different thrust and mean lift coefficients at the torque-balanced state. Therefore, for highest efficiency in forward flight as a propulsor, where profile losses begin to dominate overall efficiency, the blade planforms and airfoil sections on the front and rear proprotors may not be the same if the blades are to produce the distributions of lift coefficients that minimize profile losses at the sectional Mach and Reynolds numbers appropriate to the design conditions. Appropriate margins must also be included to retain robustness in the resulting design.

4) The issue of establishing a performance metric for best comparing the combined hovering and propulsive efficiency of a coaxial proprotor has also been discussed. A new metric was proposed based on a thrust-sharing ratio between the upper and lower rotors, reflecting the fact that each proprotor operates at a different individual efficiency across its entire operational envelope. Further work, however, must be done to explore and confirm the validity of this or any other such efficiency metric.

Acknowledgments

This work was initially supported by a subcontract award from the Army Aviation Applied Technology Directorate (AATD) and completed under a contract from the Office of Naval Research (ONR). The author is grateful for the discussions with many professional colleagues and for their advice during the course of this study. The author also appreciates the contributions of Shreyas Ananthan to this work. The comments and suggestions of the three anonymous reviewers of this paper are gratefully acknowledged. Any opinions, findings, conclusions, or recommendations expressed in this publication are those of the author alone and do not necessarily reflect the views of the University of Maryland, the sponsoring agencies, or any other organization or persons with which the author may have been associated.

References

[1]Johnson, W., Yamauchi, G. K., and Watts, M. E., "Heavy Lift Rotorcraft Systems Investigation," NASA/TP-2005-213467, December 2005. See also: Design and Technology Requirements for Civil Heavy Lift Rotorcraft, AHS San Francisco Bay Area Chapter Specialists' Conference on Vertical Lift Aircraft Design, San Francisco, CA, January 18–20, 2006.

[2]Howard, W. B., Jr., and Pilling, D. L., "Defense Science Board Task Force on Future Need for VTOL/STOL Aircraft," Defense Science Board, Washington, DC, July 2007.

[3]Gillmore, K. B., and Schneider, J. J., "Design Considerations of the Heavy Lift Helicopter," *Journal of the American Helicopter Society*, Vol. 8, (1), 1963, pp. 31–37.

[4]Wax, C. M., and Torci, R. C., "Study of the Heavy-Lift Helicopter Rotor Configuration," USAAVLABS Technical Report 66-61, November 1966.

[5]Schneider, J. J., "The Influence of Propulsion Systems on Extremely Large Helicopter Design," Paper No. 334, American Helicopter Society 25th Annual National Forum Proceedings, Washington, DC, May 16–18, 1969. See also the *Journal of the American Helicopter Society*, Vol. 15, (1), January 1970.

[6]Schneider, J. J., "The Developing Technology and Economics of Large Helicopters," Sixth European Rotorcraft and Powered Lift Aircraft Forum Proceedings, Bristol, UK, September 16–18, 1980.

[7]Schrage, D. P., Costello, M. F., and Mittlevden, D. N., "Design Concepts for an Advanced Cargo Rotorcraft," Paper AIAA-88-4496, AIAA/AHS/ASEE Aircraft Design, Systems and Operations Meeting Proceedings, Atlanta, GA, September 1988.

[8]Preator, R., Leishman, J. G., and Baldwin, G. D., "Conceptual Design Studies of a Mono Tiltrotor (MTR) Architecture," American Helicopter Society 60th Annual Forum Proceedings, Baltimore, MD, June 7–10, 2004.

[9]Preator, R., Leishman, J. G., and Baldwin, G. D., "Performance and Trade Studies of Mono Tiltrotor Design," American Helicopter Society 61st Annual Forum Proceedings, Grapevine, TX, June 1–3, 2005.

[10]Leishman, J. G., and Ananthan, S., "Aerodynamic Optimization of a Coaxial Proprotor," American Helicopter Society 62nd Annual Forum Proceedings, Phoenix, AZ, May 9–11, 2006.

[11]Samsock, J., and Leishman, J. G., "Analysis of the Aerodynamically Deployable Wings of the Mono Tiltrotor," American Helicopter Society 63rd Annual Forum Proceedings, Virginia Beach, VA, May 1–3, 2007.

[12]Farrell, M. K. "Aerodynamic Design of the V-22 Osprey Proprotor," American Helicopter Society 45th Annual Forum Proceedings, Boston, MA, May 22–24, 1989.

[13]Harris, F. D., "Performance Analysis of Two Early NACA High Speed Propellers with Application to Civil Tiltrotor Configurations," A-962481; NAS 1.26:196702; NASA-CR-196702, August 1996.

[14]Stack, J., Draley, E. C., Delano, J. B., and Feldman, L., "Investigation of the NACA 4-(3)(08)-03 and NACA 4-(3)(08)-045 Two-Blade Propellers at Forward Mach Numbers to 0.725 to Determine the Effects of Compressibility and Solidity on Performance," NACA Report 999, January 1944.

[15]Carmel, M. M., and Robinson, H. L., "Further Investigation of NACA 4-(5)(08)-03 Two-Blade Propeller at High Forward Speeds," NACA-RM-L7E12, Declassified, December 14, 1953; NACA Research Memorandum L7E12.

[16]Kim, H. W., and Brown, R. E., "Coaxial Rotor Performance and Wake Dynamics in Steady and Manoeuvring Flight," American Helicopter Society 62nd Annual Forum Proceedings, Phoenix, AZ, May 9–11, 2006.

[17]Lakshminarayan, V. K., and Baeder, J. D., "Computational Investigation of Coaxial Rotor Aerodynamics in Hover," AHS Aeromechanics Specialist's Conference Proceedings, San Francisco, CA, January 23–25, 2008.

[18]Sankar, L., "Computational Studies of Single and Counter-Rotating Propeller Configurations," 34th European Rotorcraft Forum Proceedings, Liverpool, UK, September 16–19, 2008.

[19]Weick, F. E., *Aircraft Propeller Design*, McGraw–Hill Book Co., Inc., New York, NY, 1930.

[20]Froude, W., "On the Elementary Relation between Pitch, Slip and Propulsive Efficiency," *Transactions of the Institute of Naval Architects*, 19, 1878, pp. 47–57.

[21]Gessow, A., "Effect of Rotor-Blade Twist and Plan-Form Taper on Helicopter Hovering Performance," NACA Technical Note 1542, 1948.

[22]Gessow, A., and Myers, G. C., *Aerodynamics of the Helicopter*, McMillan Co., New York, NY, 1952, pp. 73–75.

[23]Leishman, J. G., *Principles of Helicopter Aerodynamics*, 2nd edition, Cambridge University Press, New York, NY, 2006.

[24]Johnson, W., *Helicopter Theory*, Princeton University Press, Princeton, NJ, 1980.

[25]Leishman, J. G., and Ananthan, S., "An Optimum Coaxial Rotor System for Axial Flight," *Journal of the American Helicopter Society*, Vol. 53, (4), October 2008, pp. 366–381.

[26]Lock, C. N. H., "Interference Velocity for a Close Pair of Contra-Rotating Airscrews," British R&M No. 2084, July 1941.

[27]Playle, S. C., Korkan, K. D., and von Lavante, E., "A Numerical Method for the Design and Analysis of Counter-Rotating Propellers," *Journal of Propulsion and Power*, Vol. 2, (1), January–February 1986, pp. 57–53.

[28]Davidson, R. E., "Optimization and Performance Calculation of Dual-Rotation Propellers," NASA TP 1948, December 1981.

[29]Leishman, J. G., and Syal, M., "Figure of Merit Definition for Coaxial Rotors," *Journal of the American Helicopter Society*, Vol. 53, (3), July 2008, pp. 290–300.

[30]Evans, A. J., and Liner, G., "Wind Tunnel Investigation of the Aerodynamic Characteristics of a Full-Scale Supersonic-Type Three-Blade Propeller at Mach Numbers to 0.96," NACA Report 1375, May 1958.

[31]Coleman, C. P., "A Survey of Theoretical and Experimental Coaxial Rotor Aerodynamic Research," Nineteenth European Rotorcraft Forum, Cernobbio, Italy, September 14–16, 1993.

[32]Bagai, A., and Leishman, J. G., "Free-Wake Analysis of Tandem, Tilt-Rotor and Coaxial Rotor Configurations," *Journal of the American Helicopter Society*, Vol. 41, (3), 1996, pp. 196–207.

[33]Bhagwat, M. J., and Leishman, J. G., "Stability, Consistency and Convergence of Time-Marching Free-Vortex Rotor Wake Algorithms," *Journal of the American Helicopter Society*, Vol. 46, (1), January 2001, pp. 59–71.

[34]Leishman, J. G., Bhagwat, M. J., and Bagai, A., "Free-Vortex Filament Methods for the Analysis of Helicopter Rotor Wakes," *Journal of Aircraft*, Vol. 39, (5), September–October, 2002, pp. 759–775.

[35]Biermann, D., and Hartman, E., "Wind-Tunnel Tests of Four- and Six-Bladed Single- and Dual Rotating Tractor Propellers," NACA Report 747, July 1940.

[36]Biermann, D., and Gray, W. H., "Wind-Tunnel Tests of Eight-Bladed Single- and Dual Rotating Propellers in the Tractor Position," NACA Wartime Report ARR (unclassified), November 1941.

[37]Biermann, D., Gray, W. H., and Maynard, J. D., "Wind-Tunnel Test of Single- and Dual-Rotating Tractor Propellers of Large Blade Width," NASA Wartime Report ARR (unclassified), September 1942.

[38]Naiman, I., "Method of Calculating Dual-Rotating Propellers from Airfoil Characteristics," NACA Wartime Report, ARR No. 3E24 (unclassified), May 1943.

[39]Gray, W. H., "Wind-Tunnel Tests of Dual-Rotating Propellers with Systematic Differences in the Number of Blades, Blade Setting, and Rotational Speeds of the Front and Rear Propellers," NACA Wartime Report ARR No. L4E22 (unclassified), May 1944.